USGS
science for a changing world

System Characterization Report on Planet's Dove Classic

Chapter C of
System Characterization of Earth Observation Sensors

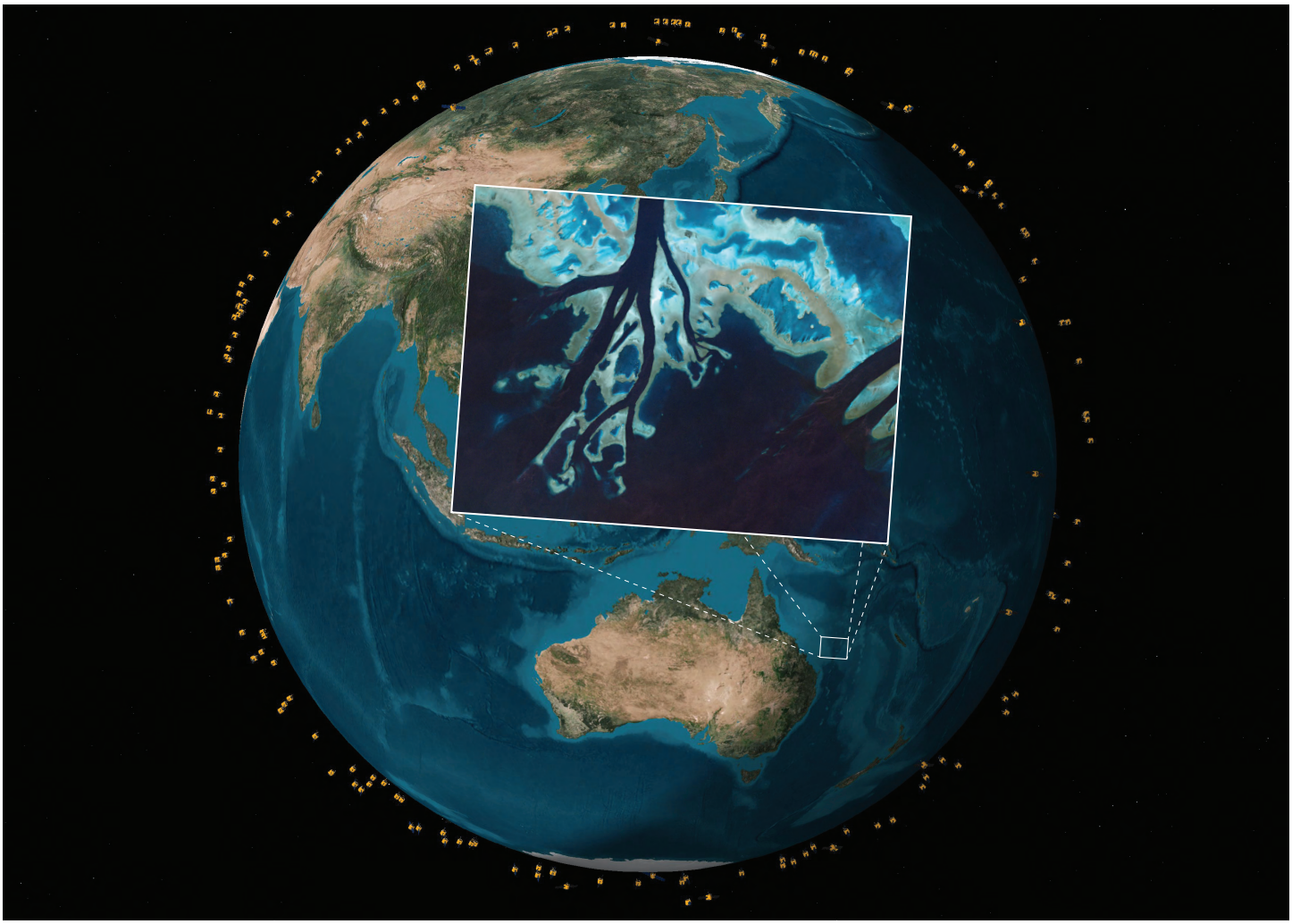

Open-File Report 2021–1030–C

U.S. Department of the Interior
U.S. Geological Survey

Cover: Satellite image of the Great Barrier Reef, Australia, taken July 8, 2016, using the Planetscope sensor. Image courtesy of Planet, licensed under the Creative Commons Attribution-NonCommercial 2.0 Generic license. An image showing the current (2021) operational Planet flock satellites, generated from Analytical Graphics, Inc., Systems Tool Kit.

System Characterization Report on Planet's Dove Classic

By Minsu Kim,[1] Seonkyung Park,[1] Cody Anderson,[2] and Gregory L. Stensaas[2]

Chapter C of
System Characterization of Earth Observation Sensors

Compiled by Shankar N. Ramaseri Chandra[1]

[1]KBR, Inc., under contract to the U.S. Geological Survey.

[2]U.S. Geological Survey.

Open-File Report 2021–1030–C

U.S. Department of the Interior
U.S. Geological Survey

U.S. Geological Survey, Reston, Virginia: 2021

Suggested citation:
Kim, M., Park, S., Anderson, C., and Stensaas, G.L., 2021, System characterization report on Planet's Dove Classic, chap. C *of* Ramaseri Chandra, S.N., comp., System characterization of Earth observation sensors: U.S. Geological Survey Open-File Report 2021–1030, 28 p., https://doi.org/10.3133/ofr20211030C.

ISSN 2331-1258 (online)

Contents

Figures

Tables

Conversion Factors

U.S. customary units to International System of Units

Multiply	By	To obtain
	Length	
inch (in.)	2.54	centimeter (cm)
inch (in.)	25.4	millimeter (mm)

International System of Units to U.S. customary units

Multiply	By	To obtain
	Length	
centimeter (cm)	0.3937	inch (in.)
meter (m)	3.281	foot (ft)
meter (m)	1.094	yard (yd)
kilometer (km)	0.6214	mile (mi)
	Mass	
kilogram (kg)	2.205	pound avoirdupois (lb)

Abbreviations

ECCOE	Earth Resources Observation and Science Cal/Val Center of Excellence
GSD	ground sample distance
JACIE	Joint Agency Commercial Imagery Evaluation
OLI	Operational Land Imager
SNR	signal-to-noise ratio
USGS	U.S. Geological Survey

System Characterization Report on Planet's Dove Classic

By Minsu Kim,[1] Seonkyung Park,[1] Cody Anderson,[2] and Gregory L. Stensaas[2]

Executive Summary

This report addresses system characterization of Planet's Dove Classic satellites and is part of a series of system characterization reports produced and delivered by the U.S. Geological Survey Earth Resources Observation and Science Cal/Val Center of Excellence. These reports present and detail the methodology and procedures for characterization; present technical and operational information about the specific sensing system being evaluated; and provide a summary of test measurements, data retention practices, data analysis results, and conclusions.

Since 2013, Planet has launched more than 360 Dove 3U CubeSats, where U stands for 10-centimeter (cm) x 10-cm x 10-cm stowed dimensions, each weighing about 5 kilograms. Since 2015, all Dove satellites have had four-band imagers with about a 4-meter (m) pixel ground sample distance. Since 2016, all Doves have been launched into Sun-synchronous orbits varying from 474 to 524 kilometers, with inclinations between 97 and 98 degrees. The Dove series satellites do not have orbit maintenance capabilities; thus, their orbits decay slowly over time, contributing to shorter lifetimes of about 3 years. More information on Planet satellites and sensors is available in the "2020 Joint Agency Commercial Imagery Evaluation—Remote Sensing Satellite Compendium" and from the manufacturer at https://www.planet.com/.

The Earth Resources Observation and Science Cal/Val Center of Excellence system characterization team completed data analyses to characterize the geometric (interior and exterior), radiometric, and spatial performances. Results of these analyses indicate that Dove Classic has an interior geometric performance in the range of −0.218 (−0.073 pixel) to −0.037 m (−0.012 pixel) in easting and −0.167 (−0.056 pixel) to −0.111 m (−0.037 pixel) in northing in band-to-band registration, an exterior geometric error of −6.841 (−2.280 pixels) in easting and −6.235 m (−2.078 pixels) in northing offset in comparison to Landsat 8 Operational Land Imager, a radiometric performance in the range of −0.057 to −0.010 in offset and 0.963 to 1.298 in slope, and a spatial perfor-mance in the range of 2.77 to 3.35 pixels for full width at half maximum, with a modulation transfer function at a Nyquist frequency in the range of 0.003 to 0.010.

[1]KBR, Inc., under contract to the U.S. Geological Survey.

[2]U.S. Geological Survey.

Introduction

Planet, Inc. is well known for launching reduced-mass Earth observation satellites, with its Dove satellites weigh-ing 5.8 kilograms (12.8 pounds). Each Dove is a 3U CubeSat, where U stands for 10-centimeter (cm) x 10-cm x 10-cm stowed dimensions. The first prototype Doves were launched in April 2013, followed by at least 20 more successful launches in the 7 years since, each carrying a flock of multiple Dove satellites, for a total of more than 360 Dove satellites launched into orbit. Planet has used this frequent launch cadence to produce at least 17 builds, or generations, of Doves with various technological and operating improvements in each build, which has resulted in continual advancement in capability in the 7 years since the launch of the first Dove. All data are provided with permission from Planet through their standard data access portal.

The data analysis results provided within this report have been derived from approved Joint Agency Commercial Imagery Evaluation (JACIE) processes and procedures. JACIE was formed to leverage resources from several Federal agencies for the characterization of remote sensing data and to share those results across the remote sensing community. More information about JACIE is available at https://www.usgs.gov/core-science-systems/eros/calval/jacie?qt-science_support_page_related_con=3#qt-science_support_page_related_con.

Purpose and Scope

The purpose of this report is to describe the specific sensor or sensing system, test its performance in three categories, complete related data analyses to quantify these performances, and report the results in a standardized document. In this chapter, the Dove Classic sensor is described. The performance testing of the system is limited to geometric, radiometric, and spatial. The scope of the geometric assessment is limited to testing the interior alignments of spectral bands against each other, and the exterior alignment is tested in reference to Landsat 8 Operational Land Imager (OLI).

The U.S. Geological Survey (USGS) Earth Resources Observation and Science Cal/Val Center of Excellence (ECCOE) project, and the associated system characterization process used for this assessment, follows the USGS Fundamental Science Practices, which include maintaining

data, information, and documentation needed to reproduce and validate the scientific analysis documented in this report. Additional information and guidance about Fundamental Science Practices and related resource information of interest to the public are available at https://www.usgs.gov/about/organization/science-support/office-science-quality-and-integrity/fundamental-science-practices. For additional information related to the report, please contact ECCOE at eccoe@usgs.gov.

System Description

This section describes the satellite and operational details and provides information about the Dove Classic sensor.

Satellite and Operational Details

The satellite and operational details for Dove Classic are listed in table 1.

Sensor(s) Information

The imaging sensor details for Dove Classic are listed in table 2. The relative spectral response for Dove Classic is shown in figure 1.

Table 1. Satellite and operational details for Planet's Dove Classic.

[cm, centimeter; NIR, near infrared; km, kilometer; °, degree; ±, plus or minus; m, meter; <, less than]

Product information	Dove Classic
Satellite and operational information	
Product name	Level 3B
Satellite name	Planet's Dove Classic
Satellite size	CubeSat 3U form factor (10 cm x 10 cm x 30 cm)
Sensor name(s)	Planetscope
Sensor type	Multispectral (blue, green, red, NIR)
Mission type	Global land-monitoring mission
Launch date	Multiple dates, beginning November 2018
Number of satellites	130 Planetscope satellites within constellation
Expected lifetime	About 6 years
Operator	Planet
Operational details	
Operating orbit	Sun-synchronous orbit
Orbital altitude range	475 km
Sensor angle altitude	98.0° inclination
Imaging time	9:30–11:30 a.m. (local solar time)
Geographic coverage	Land imaging ±81.5° lat.
Temporal resolution	Daily
Temporal coverage	2018 to present
Imaging angles	±25°
Ground sample distance(s)	3 m
Data licensing	Restricted
Data pricing	Limited free data; commercial imagery pricing
Data latency	<24 hours
Product abstract	https://www.planet.com/products/planet-imagery/
Product locator	https://www.planet.com/products/

Table 2. Imaging sensor details for Planet's Dove Classic.

[Planetscope has a swath width of 8 kilometers; µm, micrometer; m, meter; NIR, near infrared]

Spectral band(s) details	Dove Classic			
	Lower band (µm)	Upper band (µm)	Radiometric resolution (bits)	Ground sample distance (m)
Band 1—blue	0.455	0.515	12 (scaled to 16)	3
Band 2—green	0.500	0.590	12 (scaled to 16)	3
Band 3—red	0.590	0.670	12 (scaled to 16)	3
Band 4—NIR	0.780	0.860	12 (scaled to 16)	3

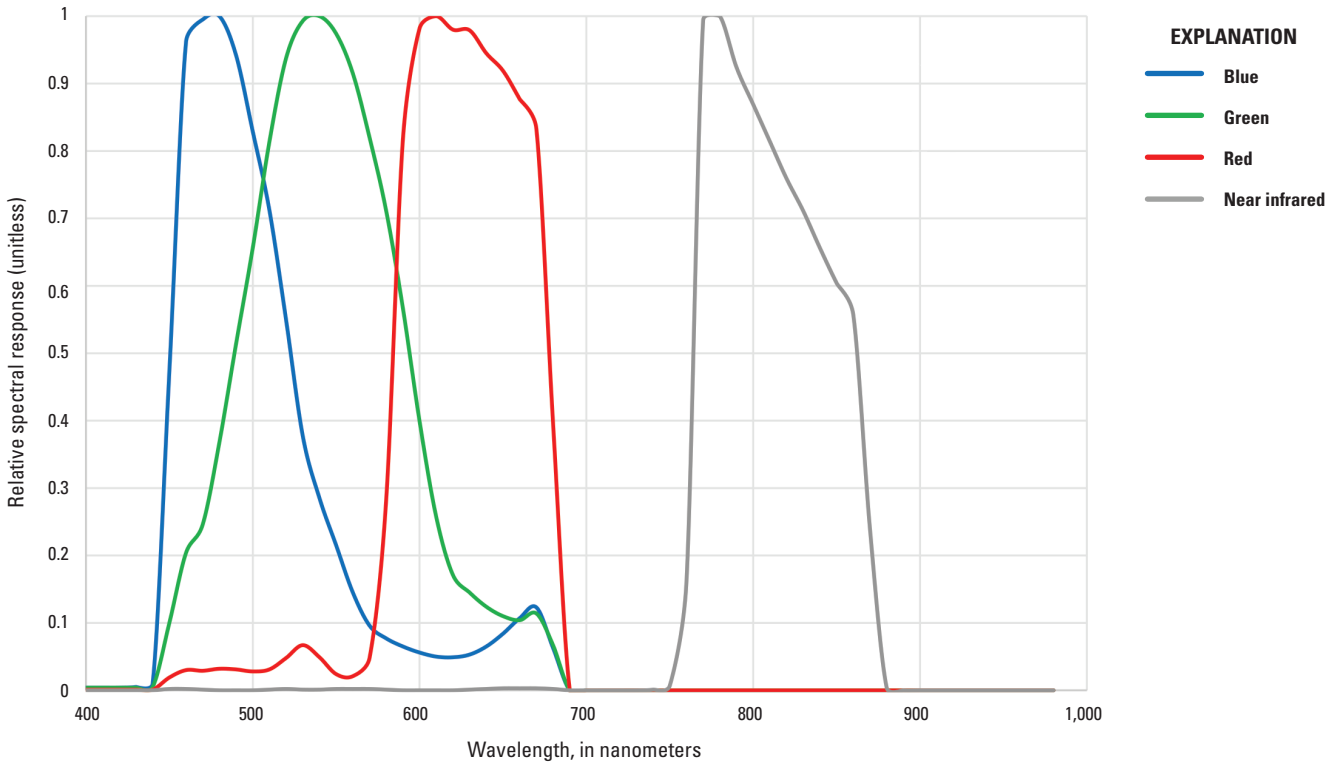

Figure 1. Planet's Dove Classic relative spectral response.

Procedures

ECCOE has established standard processes to identify Earth observing systems of interest and to assess the geometric, radiometric, and spatial qualities of data products from these systems.

The assessment steps are as follows:

- system identification and investigation to learn the general specifications of the satellite and its sensor(s);
- data receipt and initial inspection to understand the characteristics and any overt flaws in the data product so that it may be further analyzed;
- geometry characterization, including interior geometric orientation measuring the relative alignment of spectral bands and exterior geometric orientation measuring how well the georeferenced pixels within the image are aligned to a known reference;
- radiometry characterization, including assessing how well the data product correlates with a known reference and, when possible, assessing the signal-to-noise ratio (SNR); and
- spatial characterization, assessing the two-dimensional fidelity of the image pixels to their projected ground sample distance (GSD).

Data analysis and test results are maintained at the USGS Earth Resources Observation and Science Center by the ECCOE project.

Measurements

The observed USGS measurements are listed in table 3. Physical error, in meters, is calculated by the GSD multiplied by the pixel error. Details about the methodologies used are outlined in the "Analysis" section.

Analysis

This section of the report describes the geometric, radiometric, and spatial performance of Dove Classic.

Geometric Performance

The geometric performance for Dove Classic is characterized in terms of the interior (band-to-band alignment) and exterior (geometric location accuracy) geometric analysis results.

Table 3. U.S. Geological Survey measurement results.

[USGS, U.S. Geological Survey; m, meter; RMSE, root mean square error; L8 OLI, Landsat 8 Operational Land Imager; Ltyp, typical radiance; RGB, red, green, blue; ~, about; NIR, near infrared; FWHM, full width at half maximum; MTF, modulation transfer function]

Description of product	Top of Atmosphere reflectance
USGS measurement results	
Geometric performance (easting, northing), in meters (pixels)	
Interior (band to band)	Band 1 (blue) Mean: −0.037 m (−0.012), −0.167 m (−0.056) RMSE: 0.335 m (0.111), 0.408 m (0.136) Band 2 (green) Mean: −0.060 m (−0.020), −0.125 m (−0.042) RMSE: 0.336 m (0.111), 0.398 m (0.133) Band 3 (red) Mean: −0.085 m (−0.028), −0.143 m (−0.048) RMSE: 0.356 m (0.119), 0.444 m (0.148) Band 4 (near infrared) Mean: −0.218 m (−0.073), −0.111 m (−0.037) RMSE: 0.690 m (0.230), 0.738 m (0.246)
Exterior (geometric location accuracy)	Mean: −6.841 m (−2.280), −6.235 m (−2.078) RMSE: 6.930 m (2.310), 6.561 m (2.187)
Radiometric performance (offset, slope)	
Radiometric evaluation (linear regression—Dove Classic versus L8 OLI reflectance)	Band 1 (offset, slope): −0.010, 0.963 Band 2 (offset, slope): −0.029, 1.063 Band 3 (offset, slope): −0.042, 1.208 Band 4 (offset, slope): −0.057, 1.298
Radiometric stability	Overall radiometric characteristics were maintained over time (from April 2017 to March 2019). Time series of radiometric comparison in terms of slope and offset are provided in figures 14 and 15 in the "Analysis" section.
Signal-to-noise ratio (SNR) (all median at Ltyp)	Bands 1–3 (RGB): Mean SNR ~30 Band 4 (NIR): Mean SNR ~24
Spatial performance	
Spatial performance measurement	Band 1: FWHM = 2.77 pixels; MTF at Nyquist = 0.010 Band 2: FWHM = 3.07 pixels; MTF at Nyquist = 0.003 Band 3: FWHM = 3.07 pixels; MTF at Nyquist = 0.007 Band 4: FWHM = 3.35 pixels; MTF at Nyquist = 0.006
Known artifacts and quality issues	
USGS noted artifacts/quality issues	As predicted by the large line spread function (FWHM ranging from 2.77 to 3.35 pixels), the Dove Classic imagery does not have precise transition across a target edge. Low SNR could affect quantitative measurements.

Interior (Band-to-Band)

For this analysis, each band of the Dove Classic image was registered against all other bands. Results from three images were gathered in table 4 to determine the mean error and root mean square error as listed in table 3 with results represented in pixels. Greater misalignment was seen with band 4 (near infrared), likely as a result of poorer spatial quality and its spectral distinctness from bands 1–3. Together, the interior and exterior geometric analysis results, as reported in the "Interior (Band-to-Band)" and "Exterior (Geometric Location Accuracy)" sections, provide a comprehensive assessment of geometric accuracy. The band-to-band error in terms of error histograms and error distribution plot for three band combinations from the Roswell, New Mexico, scene (20180120_170400_0e2f) are presented in figures 2–7.

Exterior (Geometric Location Accuracy)

For this analysis, band 4 (infrared) of Dove Classic image (20190325_083005_0e2f_3B_AnalyticMS) and Landsat 8 OLI image (LC08_L1TP_180033_20190325_20190403_01_T1) for Izmir, Turkey, were compared to estimate relative geometric error. The results are listed in table 5 and the error grid is shown in figure 8, the error histogram and error distribution is shown in figure 9.

Radiometric Performance

For this analysis, 68 cloud-free regions of interest were selected from near-coincident Dove Classic system and Landsat 8 OLI scene pairs listed in appendix 1. Once the relative georeferencing error between Landsat 8 OLI and Dove Classic has been corrected, Top of Atmosphere reflectance values from the two sensors are extracted. The scatterplots are drawn in a way that the x-axis is the reference sensor and the y-axis is the comparison sensor. The linear regression, thus, represents Top of Atmosphere reflectance relative to that of the reference sensor. Ideally, the slope should be near unity and the offset should be near zero. For example, if the slope is greater than unity, that means the comparison sensor has a tendency to overestimate Top of Atmosphere reflectance compared to the reference sensor. Top of Atmosphere reflectance comparison results are listed in table 6. The range of linear regressions coefficients for four bands using all scene pairs (appendix 1) are presented. Several selected radiometric comparison graphs using Landsat 8 OLI and Dove Classic scene pairs are shown in figures 10–13.

Radiometric Stability

For this analysis, figure 14 shows a time series of the slope of the radiometric comparison between Landsat 8 OLI and Dove Classic, as calculated. A time series of the offset of

Table 4. Band-to-band registration error (in pixels).

[ID, identifier; RMSE, root mean square error]

Scene ID	Band combination	Mean error (easting)	Mean error (northing)	RMSE (easting)	RMSE (northing)
20180120_170400_0e2f (Roswell, New Mexico)	Band 1–band 2	0.007	−0.025	0.042	0.059
	Band 1–band 3	0.019	−0.062	0.058	0.101
	Band 1–band 4	−0.072	0.054	0.198	0.230
	Band 2–band 3	0.012	−0.042	0.065	0.088
	Band 2–band 4	−0.086	0.078	0.202	0.234
	Band 3–band 4	−0.119	0.115	0.207	0.246
20180303_160129_0e2f (Chicago, Illinois)	Band 1–band 2	0.008	−0.026	0.054	0.073
	Band 1–band 3	0.005	−0.076	0.067	0.114
	Band 1–band 4	−0.028	−0.077	0.266	0.237
	Band 2–band 3	−0.007	−0.053	0.072	0.099
	Band 2–band 4	−0.060	−0.079	0.255	0.254
	Band 3–band 4	−0.096	−0.066	0.256	0.255
20170708_172421_0e2f (Florence, Arizona)	Band 1–band 2	0.007	−0.043	0.038	0.053
	Band 1–band 3	0.003	−0.099	0.055	0.107
	Band 1–band 4	−0.059	−0.146	0.228	0.251
	Band 2–band 3	0.001	−0.061	0.054	0.075
	Band 2–band 4	−0.061	−0.125	0.225	0.260
	Band 3–band 4	−0.074	−0.084	0.233	0.247

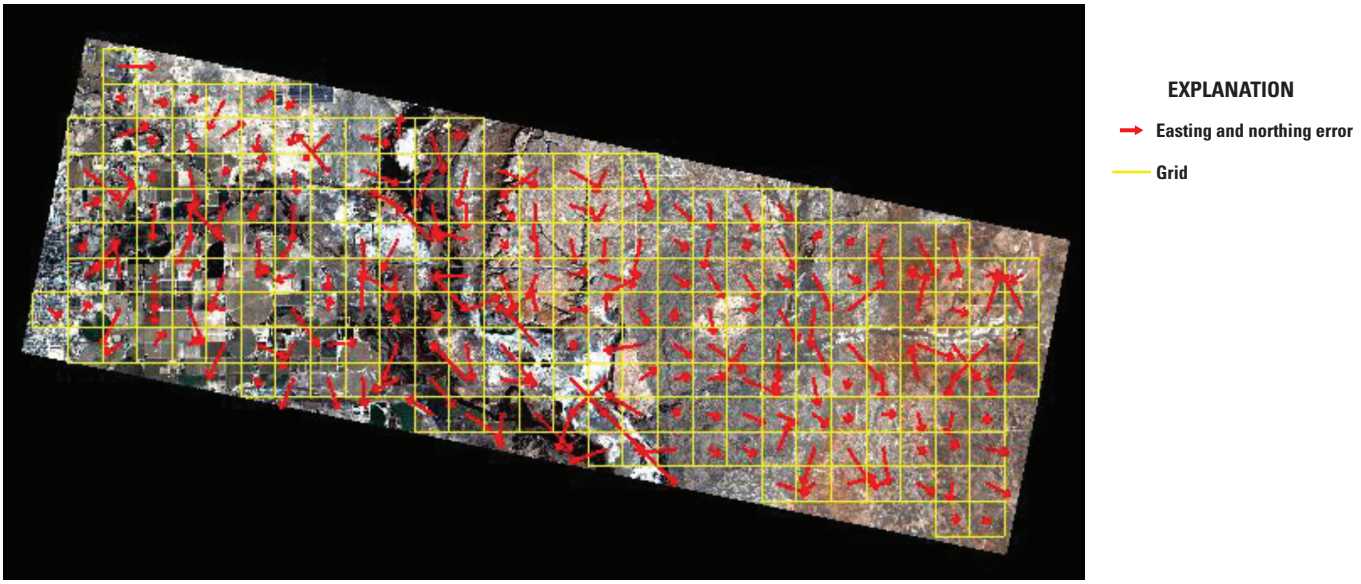

Figure 2. Band 1 (blue) to band 2 (green) geometric error map of Roswell, New Mexico.

the radiometric comparison between Landsat 8 OLI and Dove Classic is shown in figure 15. The datasets used to populate the time-series analysis results are detailed in appendix 1.

Signal-to-Noise Ratio

The SNR was calculated using homogeneous areas adjacent to an edge target over the Baotou (China) Cal/Val site. The difference between the dark and bright area pixel values (commonly measured in terms of digital numbers) is divided by the one-sigma standard deviation noise level to get the SNR. SNR results are listed in table 3.

Spatial Performance

For this analysis, edge spread and line spread functions were calculated with resulting full width at half maximum and modulation transfer function at Nyquist frequency analysis output, as listed in table 7. The Dove-Classic image for the Baotou, China, Cal/Val site used for the analysis is "20200718_031215_0f28_3B_AnalyticMS.tif" and is shown in figure 16. The band 1 (blue) edge spread and line spread function results using the Baotou (China) Cal/Val site for analysis are shown in figure 17. The yellow box in figure 16 shows the edge transect bounding box. The results for band 1 (blue) are shown in figures 17 and 18. In figure 17, the dotted lines with diamond symbols are the raw transects. The green line is the middle transect, where the red dots are the region of the curve that is used for alignment. The lower plot in figure 17 is the aligned curve and the green line represents edge spread function. In the upper plot in figure 18, a white curve is an edge spread function with red line segment shows relative edge response; the green curve is a line spread function with a white line segment represents full width at half maximum. The lower plot in figure 18 is a modulation transfer function up to Nyquist frequency (0.5) and the dashed line shows the frequency corresponding to the 50-percent modulation transfer function value. The results for band 2 (green) are shown in figures 19 and 20, the results for band 3 (red) are shown in figures 21 and 22, and the results for band 4 (near infrared) are shown in figures 23 and 24.

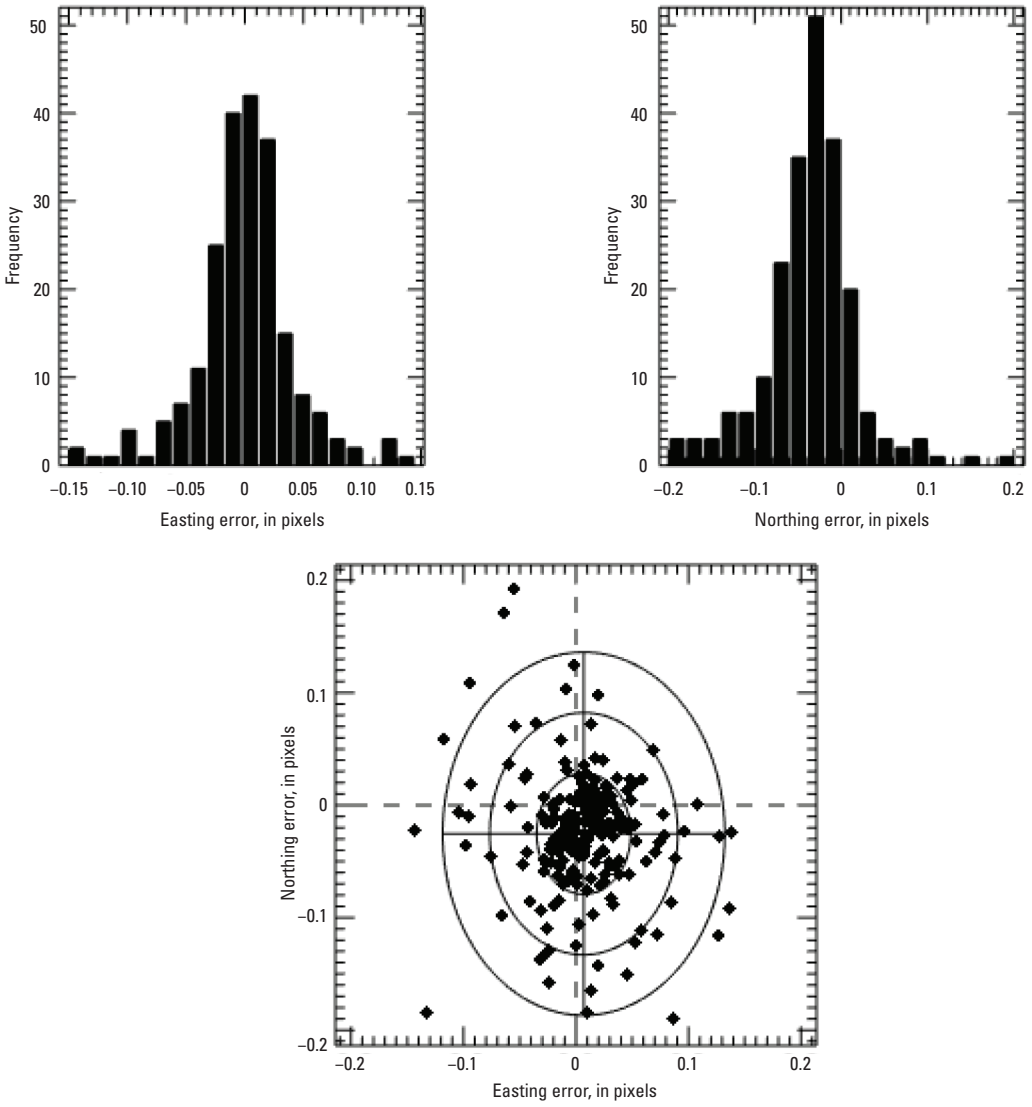

Figure 3. Band 1 (blue) to band 2 (green) geometric error histograms for easting and northing (upper) and error distribution (lower) for Roswell, New Mexico.

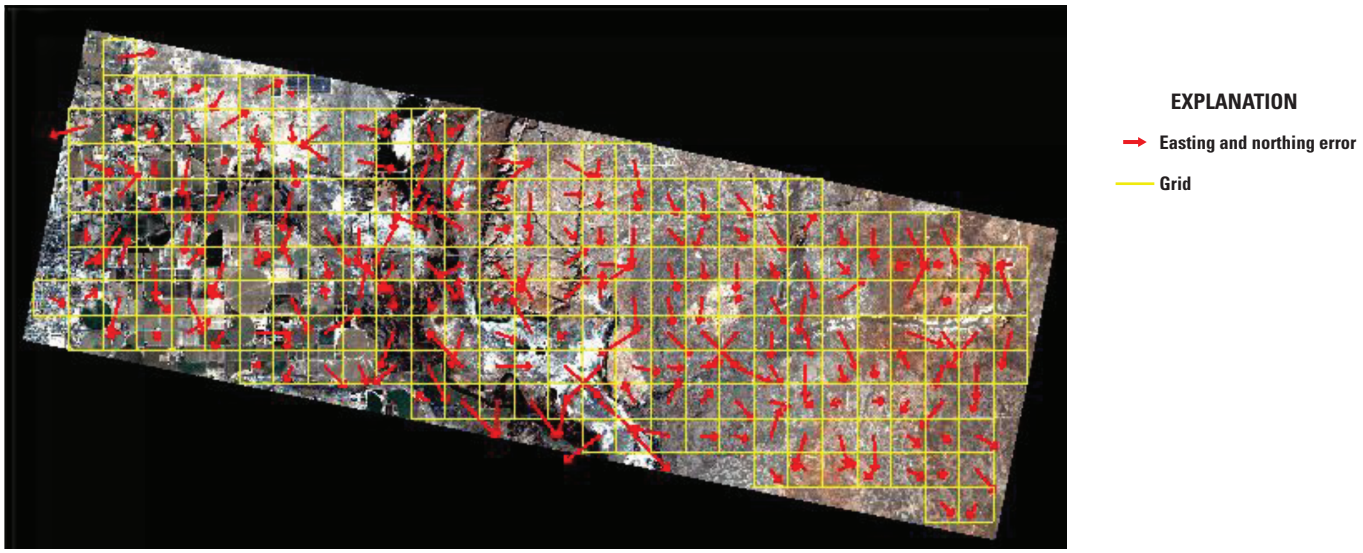

Figure 4. Band 2 (green) to band 3 (red) geometric error map of Roswell, New Mexico.

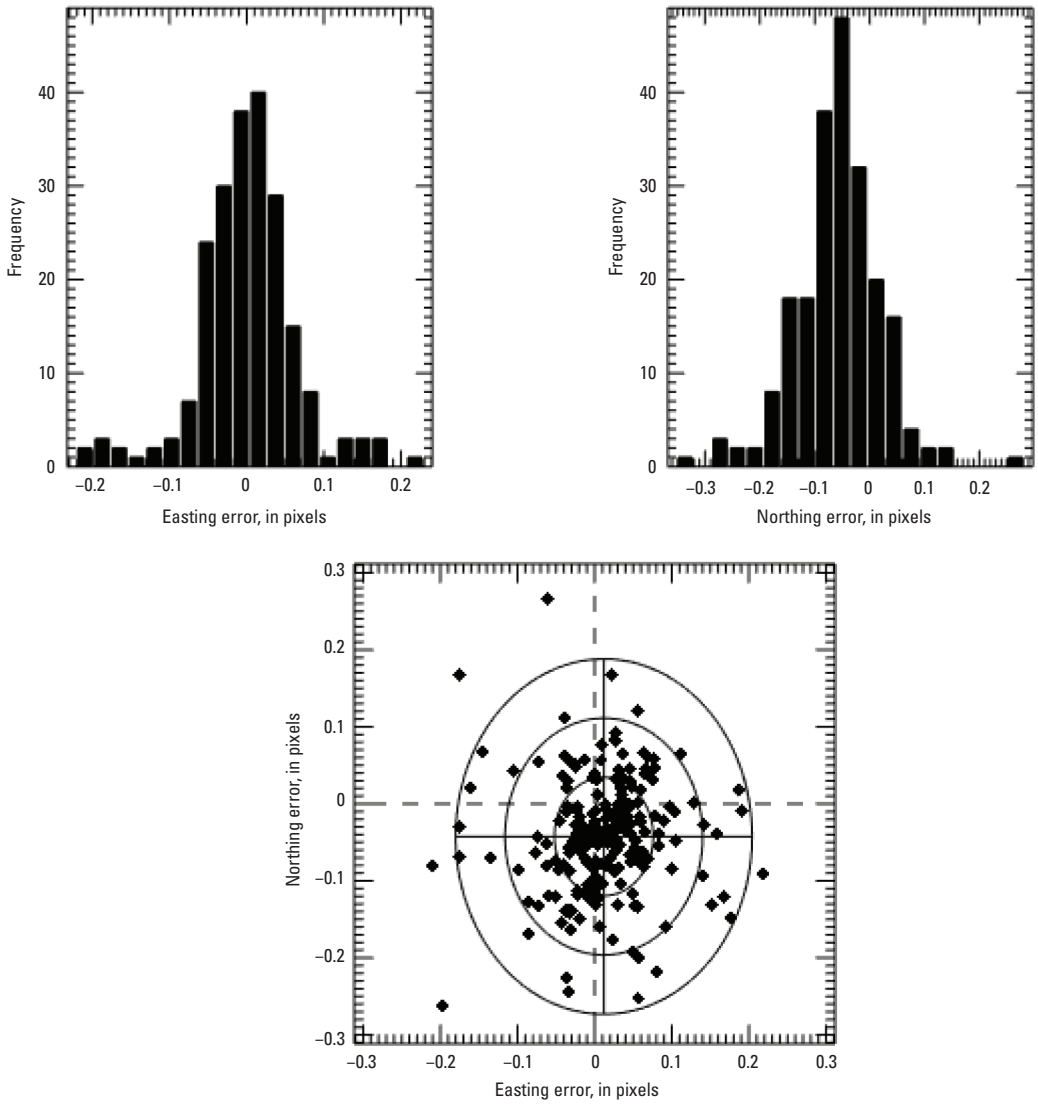

Figure 5. Band 2 (green) to band 3 (red) geometric error histograms for easting and northing (upper) and error distribution (lower) for Roswell, New Mexico.

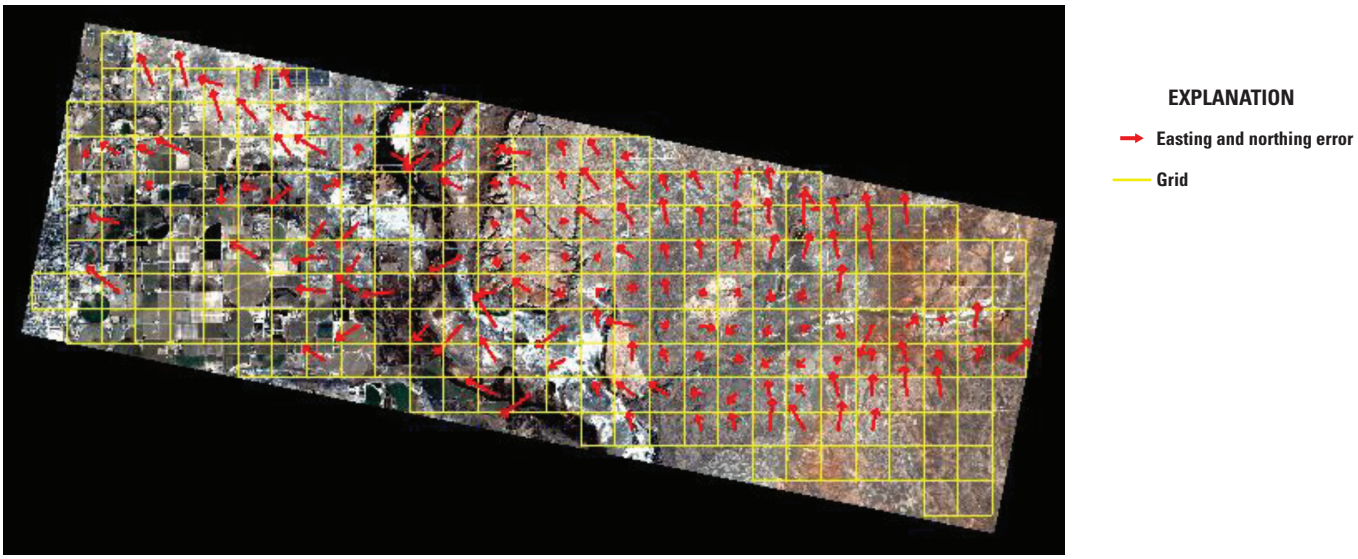

Figure 6. Band 3 (red) to band 4 (near infrared) geometric error map of Roswell, New Mexico.

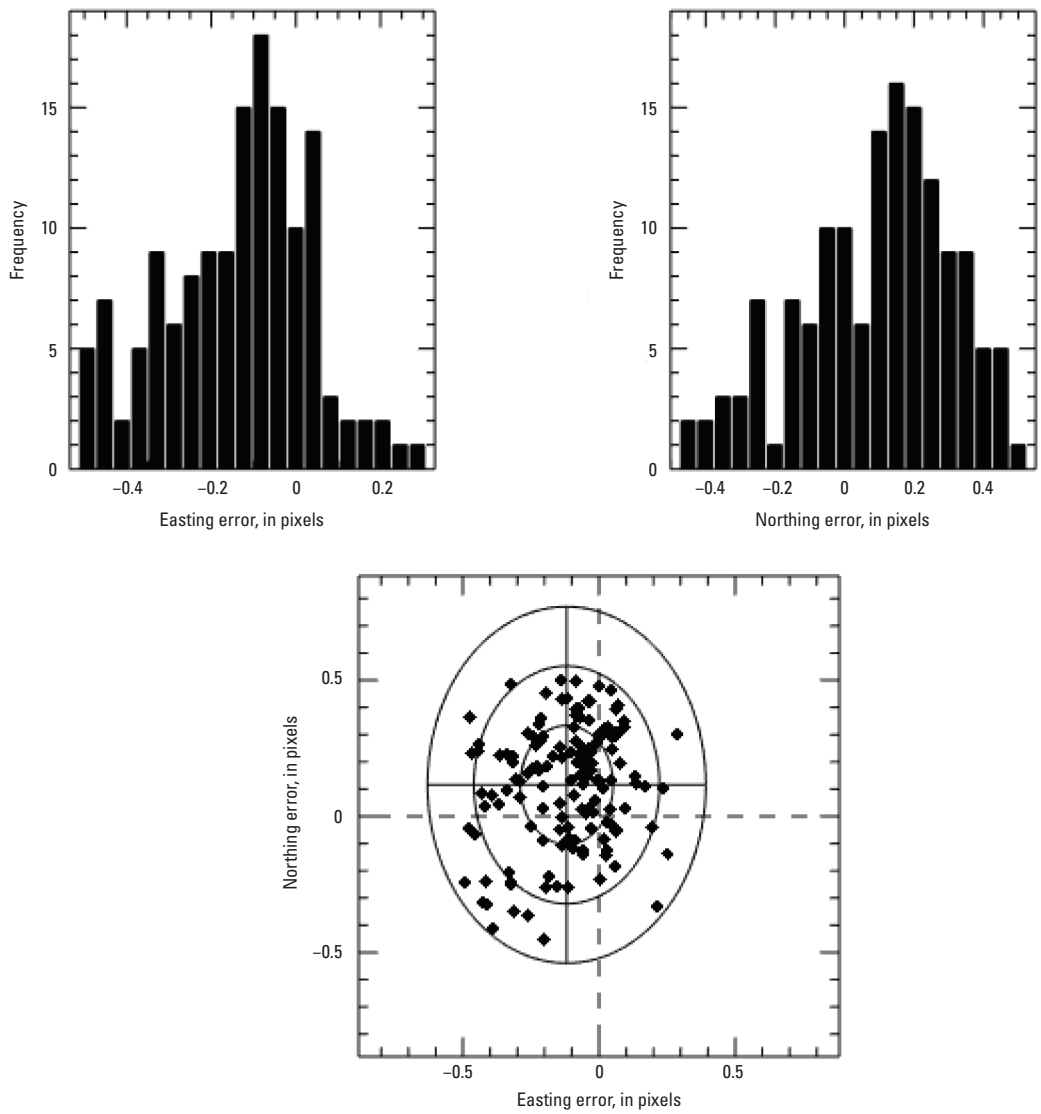

Figure 7. Band 3 (red) to band 4 (near infrared) geometric error histograms for easting and northing (upper) and error distribution (lower) for Roswell, New Mexico.

Table 5. Geometric error of Planet's Dove Classic imagery relative to Landsat 8 Operational Land Imager.

[RMSE, root mean square error; m, meter]

Mean error (easting)	Mean error (northing)	RMSE (easting)	RMSE (northing)
−2.280 pixels	−2.0781 pixels	2.310 pixels	2.187 pixels
(−6.841 m)	(−6.235 m)	(6.930 m)	(6.561 m)

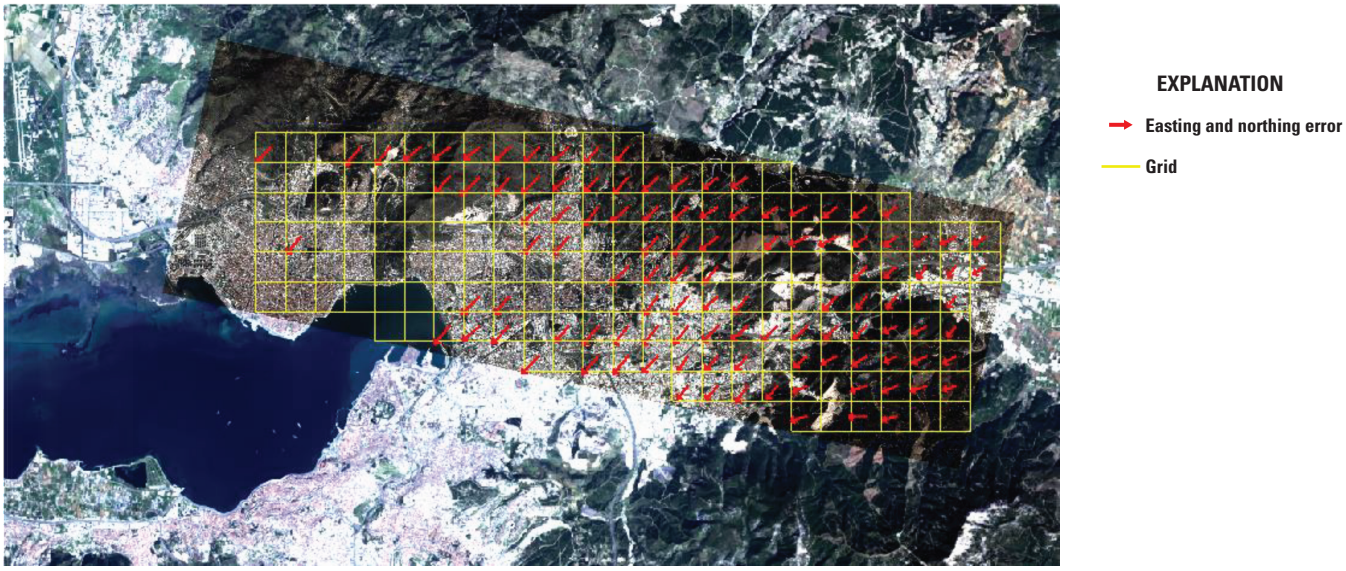

Figure 8. Relative geometric error map for Landsat 8 Operational Land Imager and Planet's Dove Classic for Izmir, Turkey.

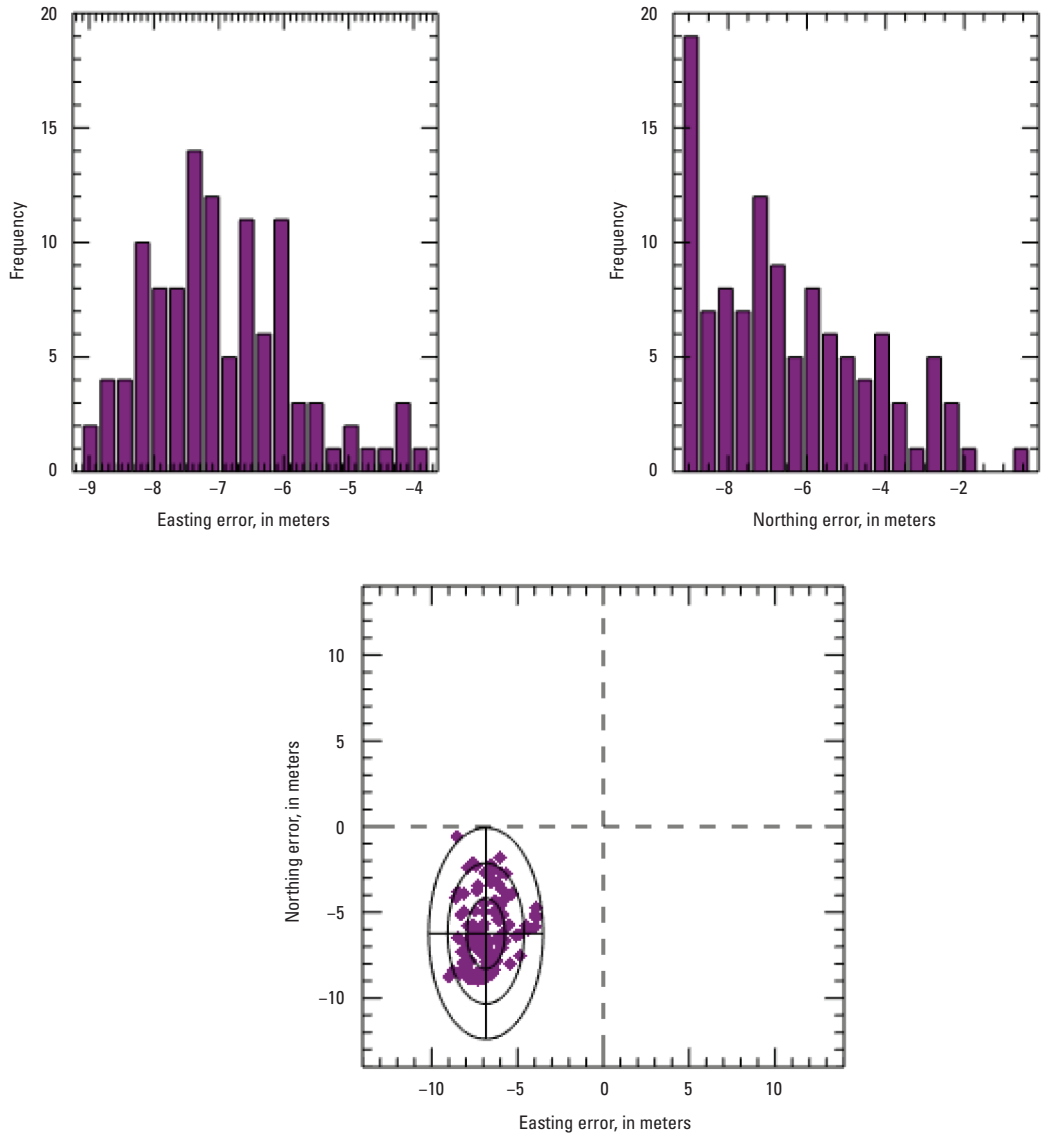

Figure 9. Relative geometric error histograms for easting and northing (upper) and error distribution (lower) for Izmir, Turkey.

Table 6. Top of Atmosphere reflectance comparison of Landsat 8 Operational Land Imager images against Planet's Dove Classic images.

[NIR, near infrared; ~, about]

Statistics	Band 1—Blue	Band 2—Green	Band 3—Red	Band 4—NIR
Radical offset	−0.021 to 0.000	−0.043 to ~0.015	−0.062 to −0.019	−0.103 to −0.025
Radical slope	0.991 to 1.114	1.081 to 1.224	1.177 to 1.409	1.282 to 1.500

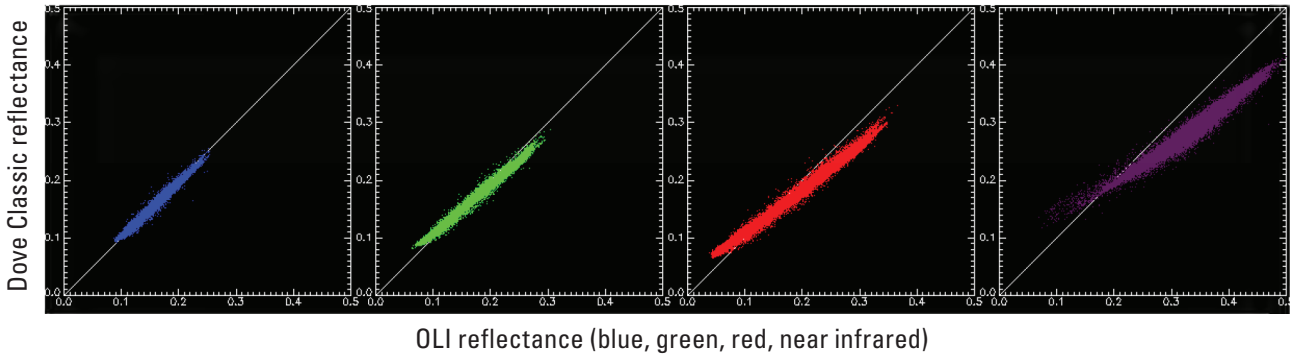

Figure 10. Top of Atmosphere reflectance comparison for Landsat 8 Operational Land Imager (OLI) and Dove Classic, April 2017 scene pair (LC08_L1TP_023037_20170408_20170414_01_T1 and 20170408_160456_0e2f_3B_AnalyticMS, respectively).

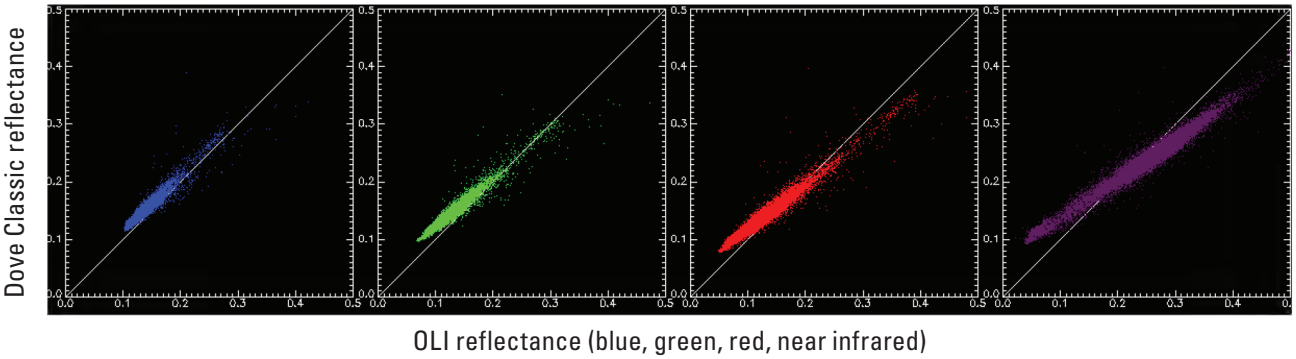

Figure 11. Top of Atmosphere reflectance comparison for Landsat 8 Operational Land Imager (OLI) and Dove Classic, December 2017 scene pair (LC08_L1TP_128049_20171220_20171224_01_T1 and 20171220_030332_0e2f_3B_AnalyticMS, respectively).

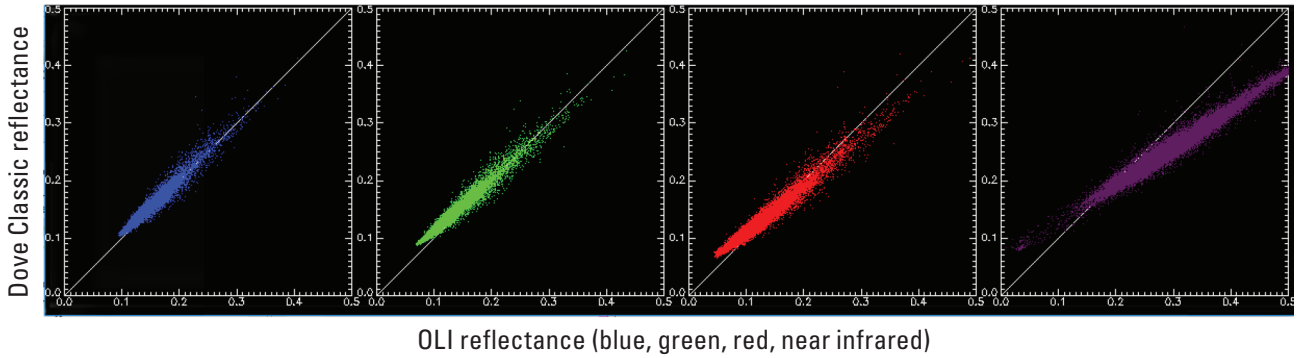

Figure 12. Top of Atmosphere reflectance comparison for Landsat 8 Operational Land Imager (OLI) and Dove Classic, August 2018 scene pair (LC08_L1TP_192029_20180817_20180829_01_T1 and 20180817_093542_0e2f_3B_AnalyticMS, respectively).

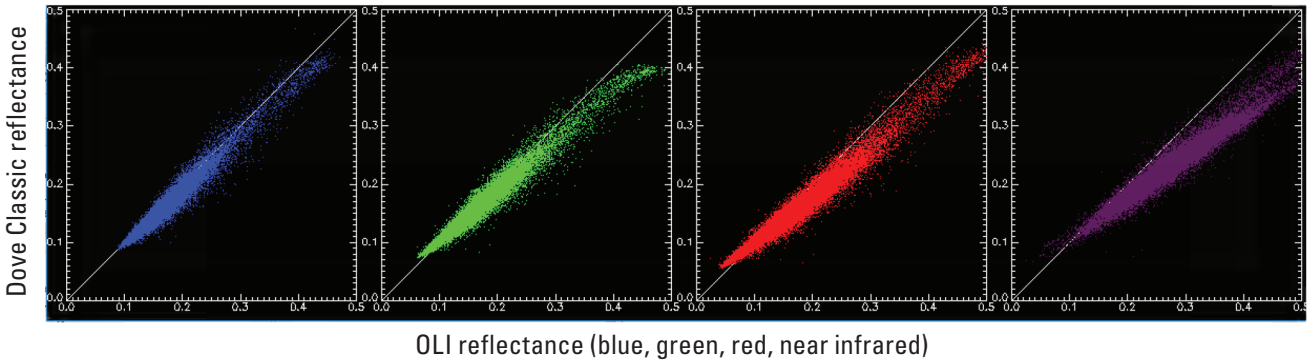

Figure 13. Top of Atmosphere reflectance comparison for Landsat 8 Operational Land Imager (OLI) and Dove Classic, March 2019 scene pair (LC08_L1TP_180032_20190325_20190403_01_T1 and 20190325_082920_0e2f_3B_AnalyticMS, respectively).

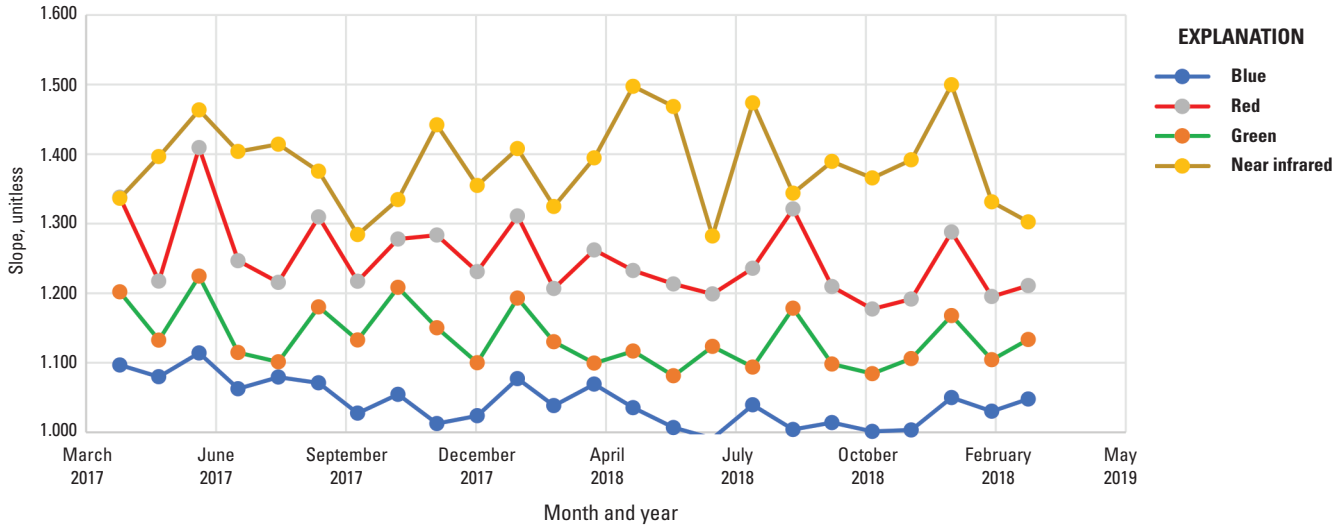

Figure 14. Time series of Landsat 8 Operational Land Imager and Planet's Dove Classic radiometric slope comparison.

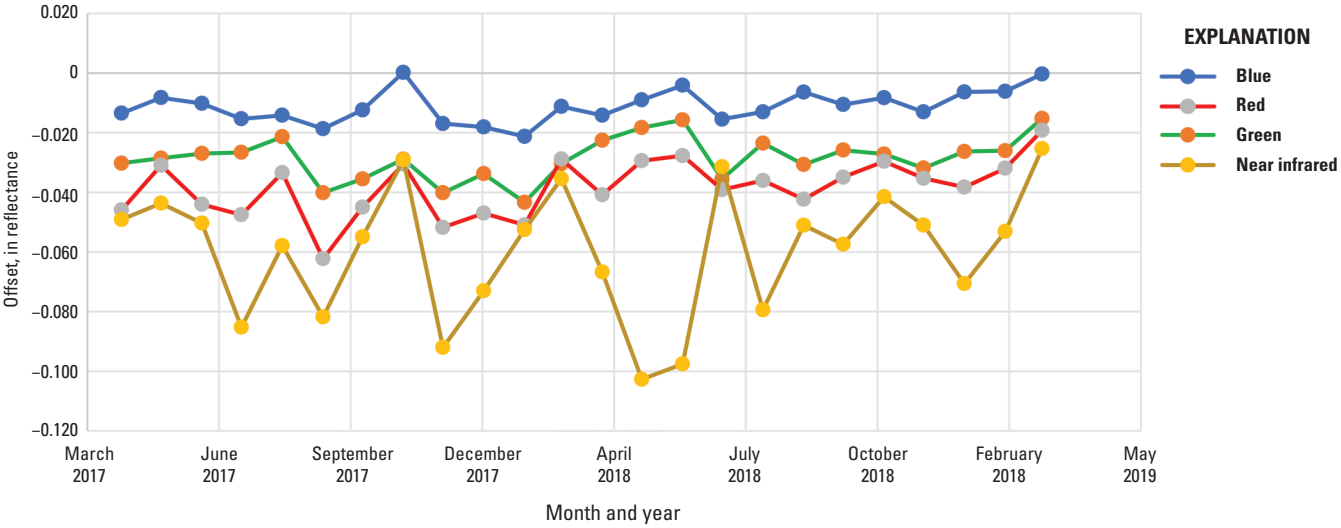

Figure 15. Time series of Landsat 8 Operational Land Imager and Planet's Dove Classic radiometric offset comparison.

Table 7. Spatial performance of Planet's Dove Classic.

[RER, relative edge response; FWMH, full width at half maximum; MTF, modulation transfer function; NIR, near infrared]

Spatial analysis	RER	FWHM	MTF at Nyquist
Band 1—blue	0.36	2.77 pixels	0.010
Band 2—green	0.33	3.07 pixels	0.003
Band 3—red	0.33	3.07 pixels	0.007
Band 4—NIR	0.27	3.35 pixels	0.006

Figure 16. Dove-Classic image of calibration site at Baotou, China.

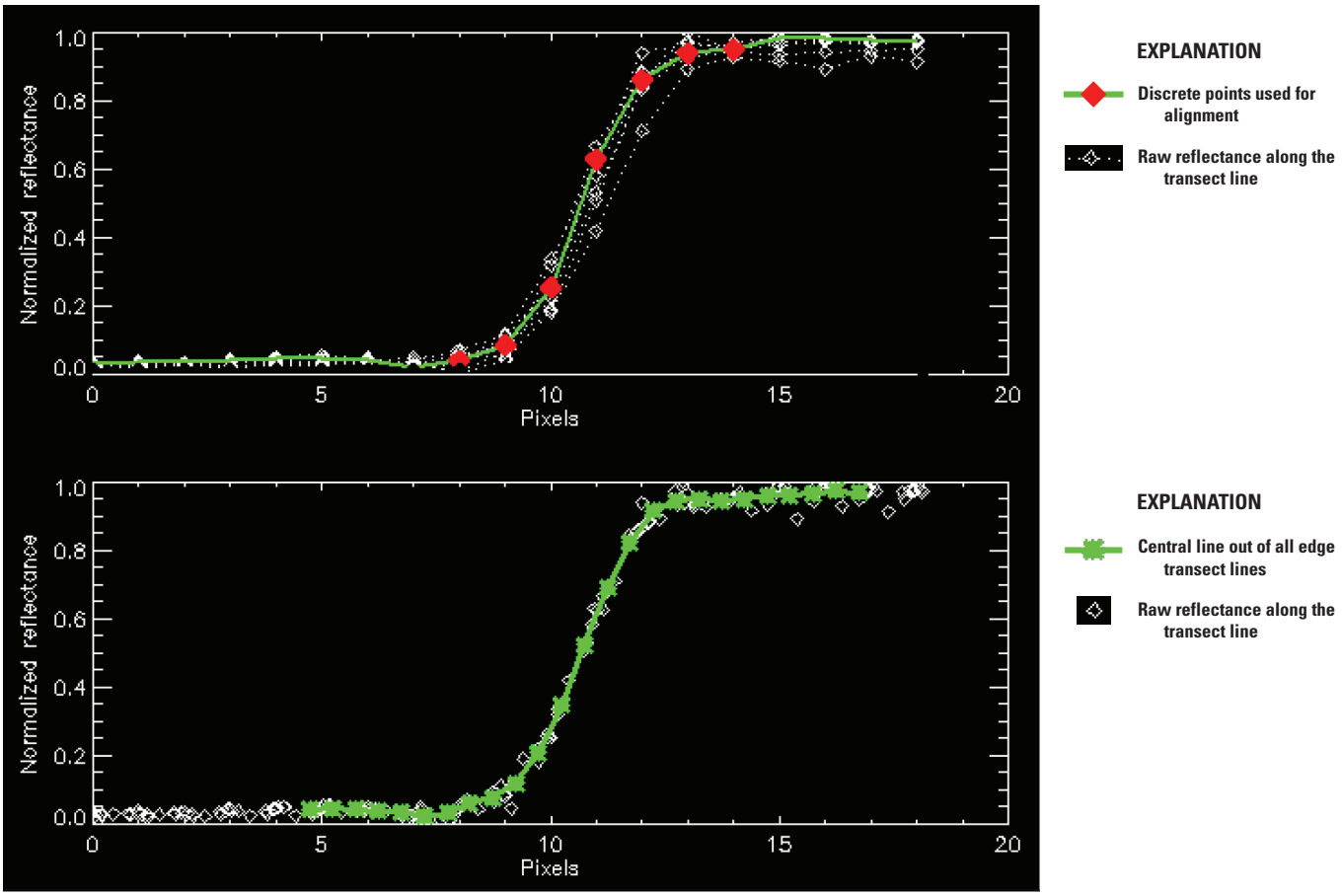

Figure 17. Band 1 (blue) raw edge transects (upper) and shifted transects (lower) for Baotou, China.

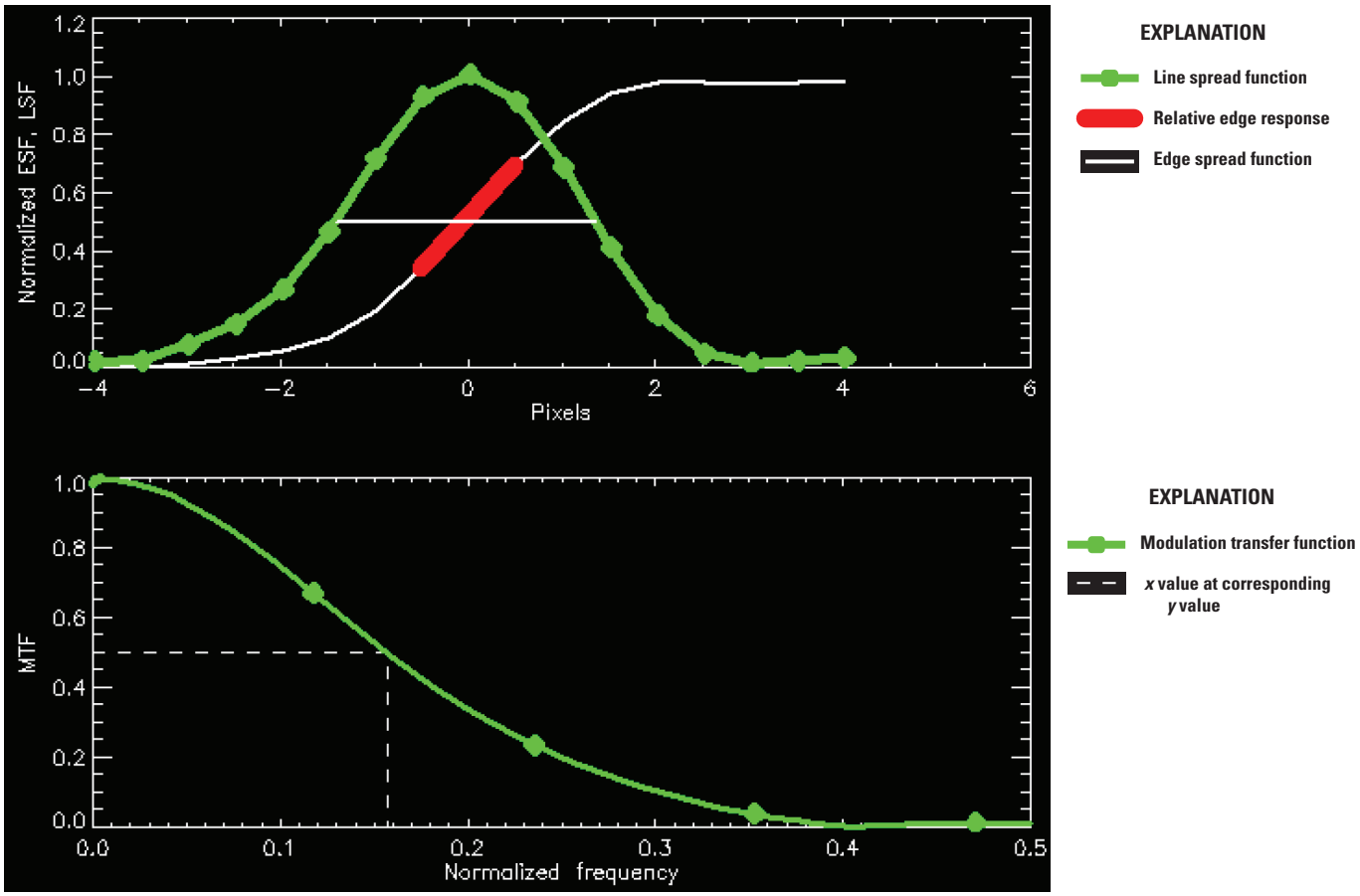

Figure 18. Band 1 (blue) edge spread function (ESF) and line spread function (LSF; upper) and modulation transfer function (MTF; lower) for Baotou, China.

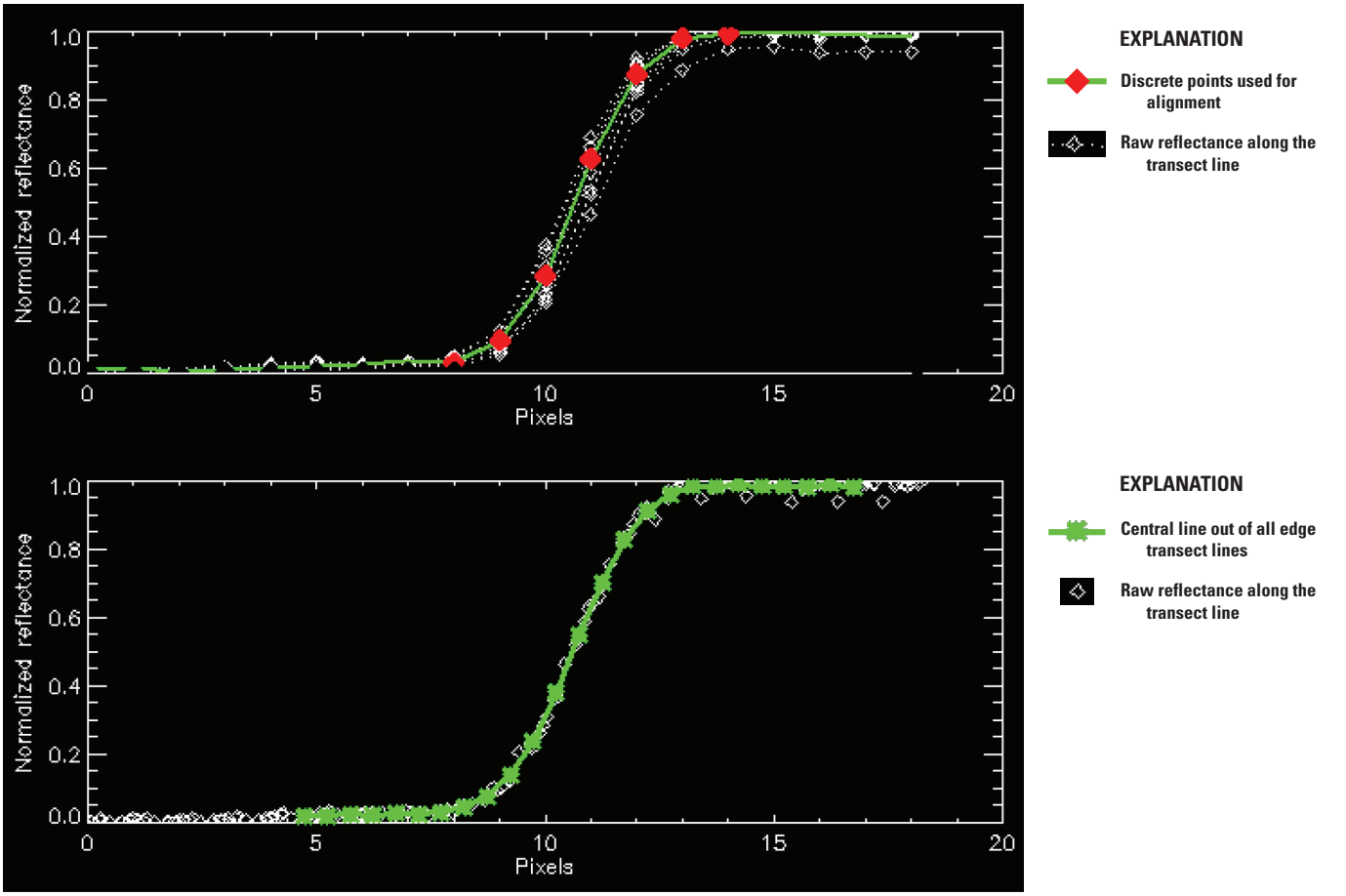

Figure 19. Band 2 (green) raw edge transects (upper) and shifted transects (lower) for Baotou, China.

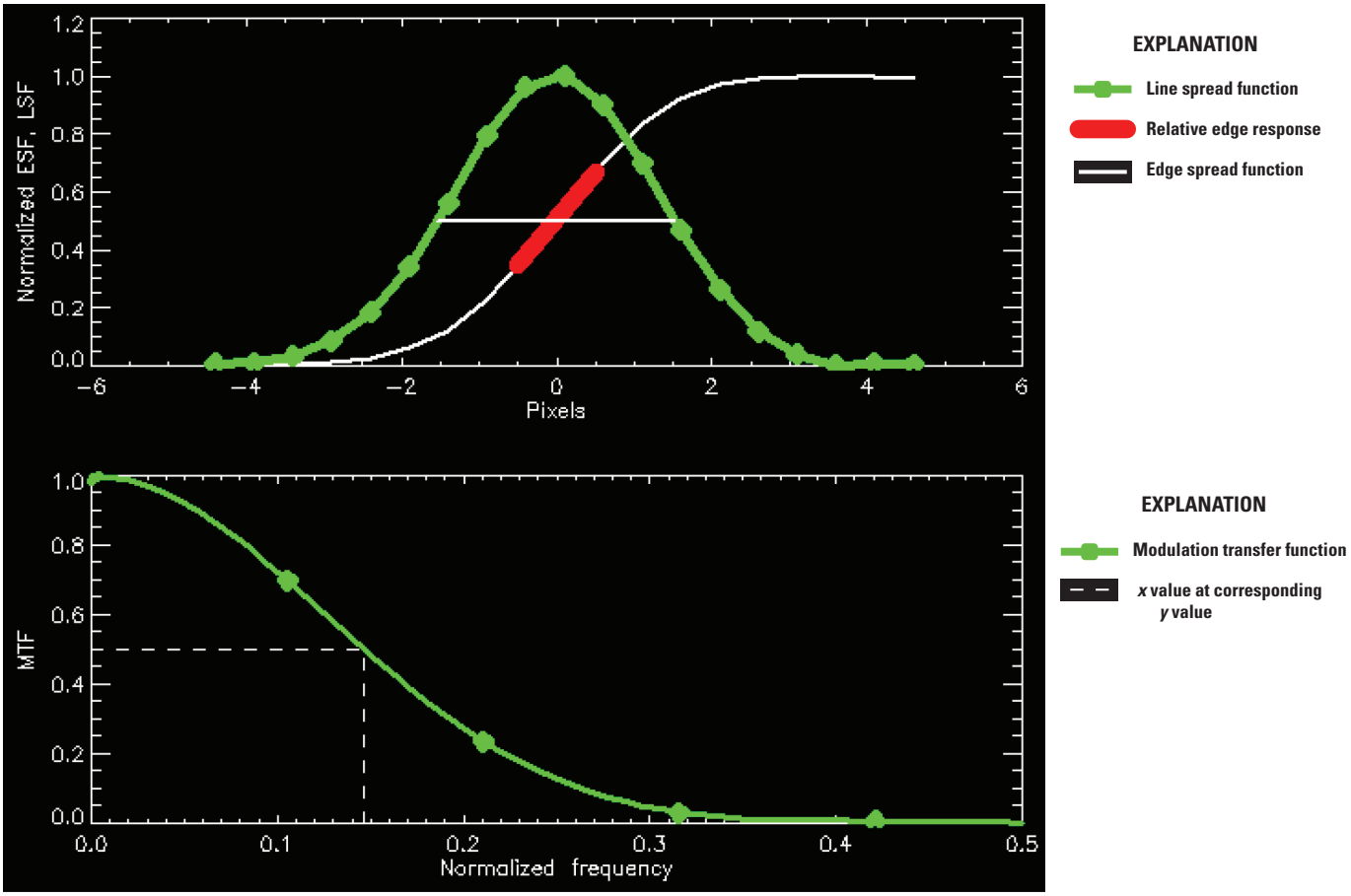

Figure 20. Band 2 (green) edge spread function (ESF) and line spread function (LSF; upper) and modulation transfer function (MTF; lower) for Baotou, China.

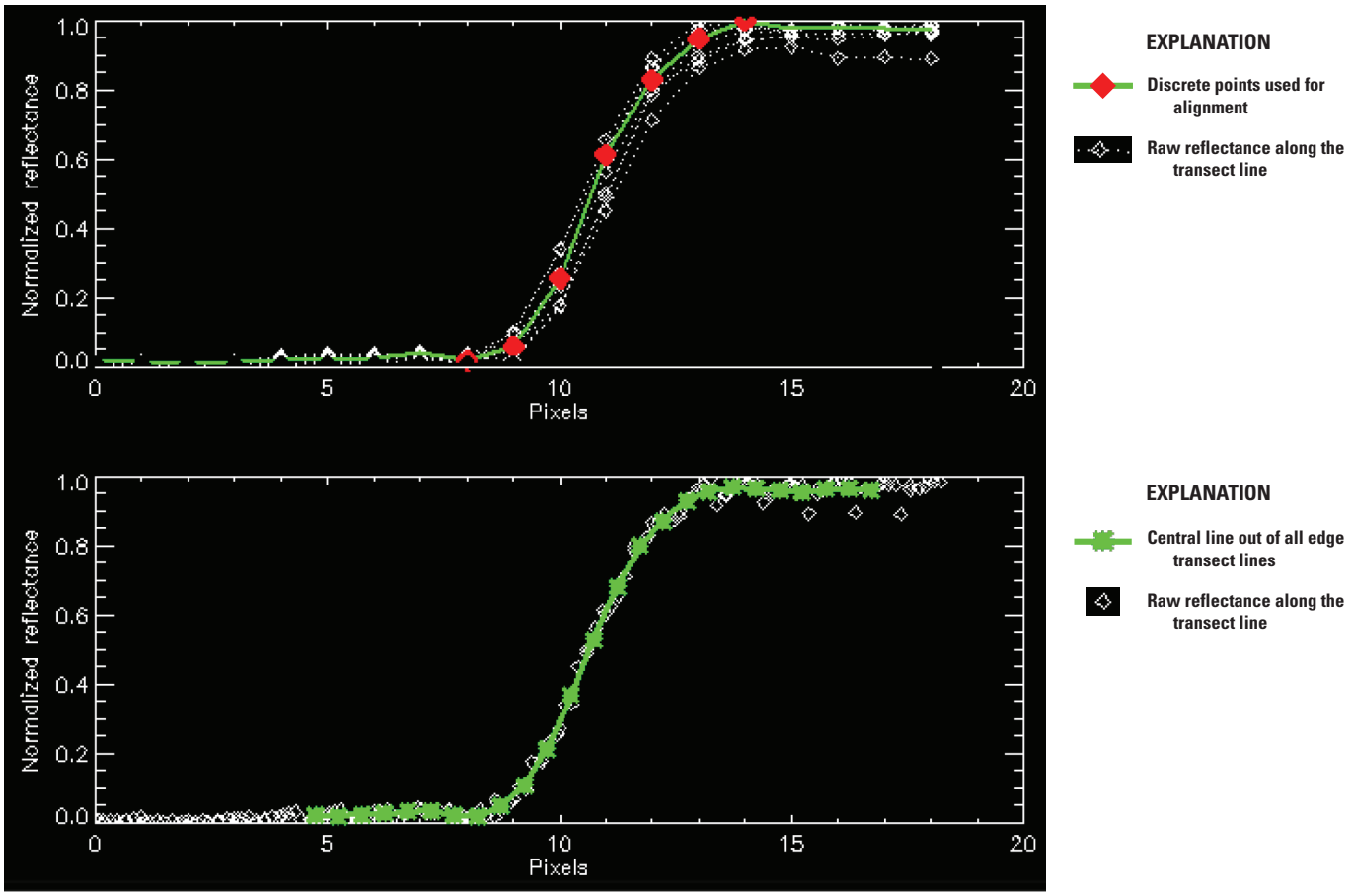

Figure 21. Band 3 (red) raw edge transects (upper) and shifted transects (lower) for Baotou, China.

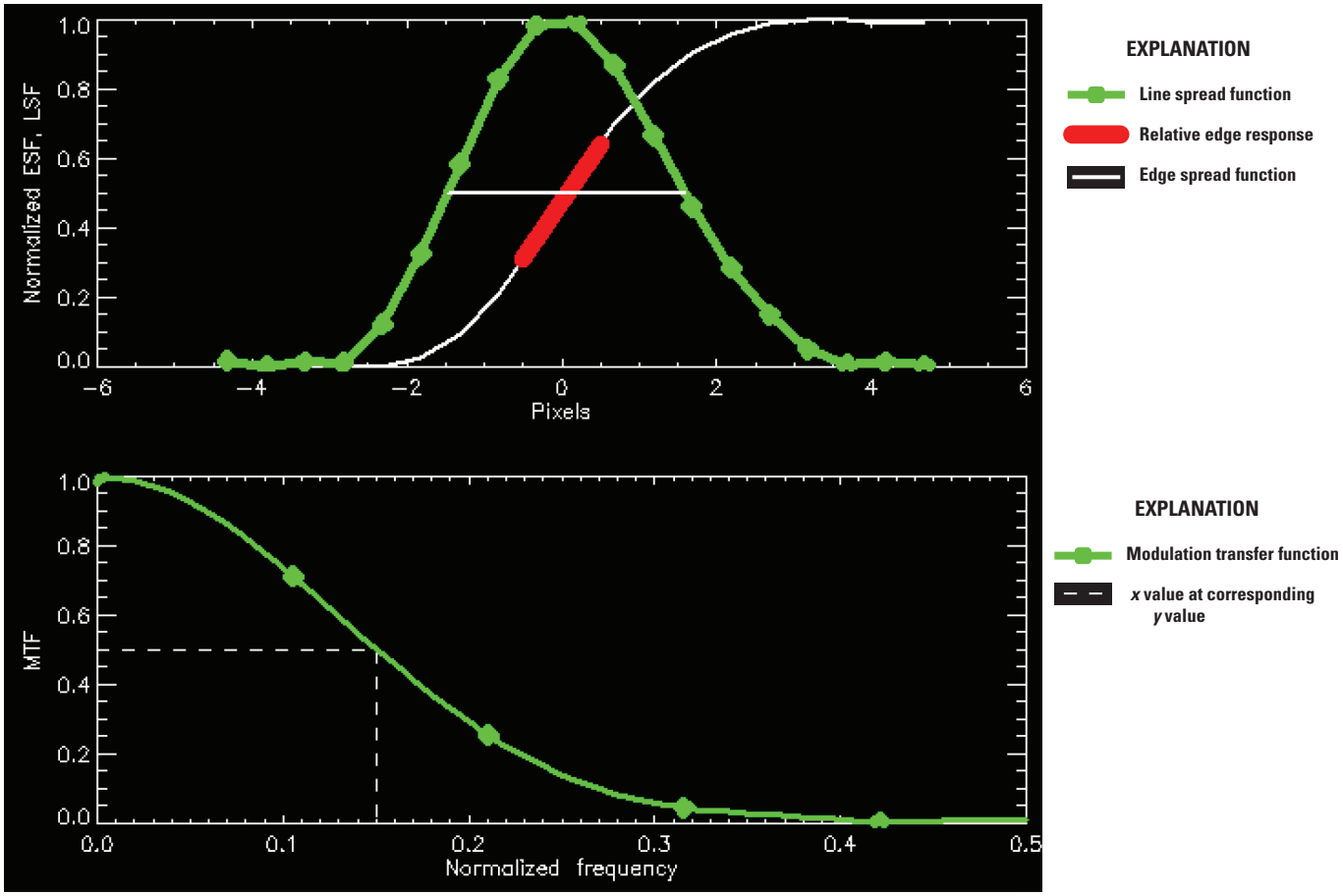

Figure 22. Band 3 (red) edge spread function (ESF) and line spread function (LSF; upper) and modulation transfer function (MTF; lower) for Baotou, China.

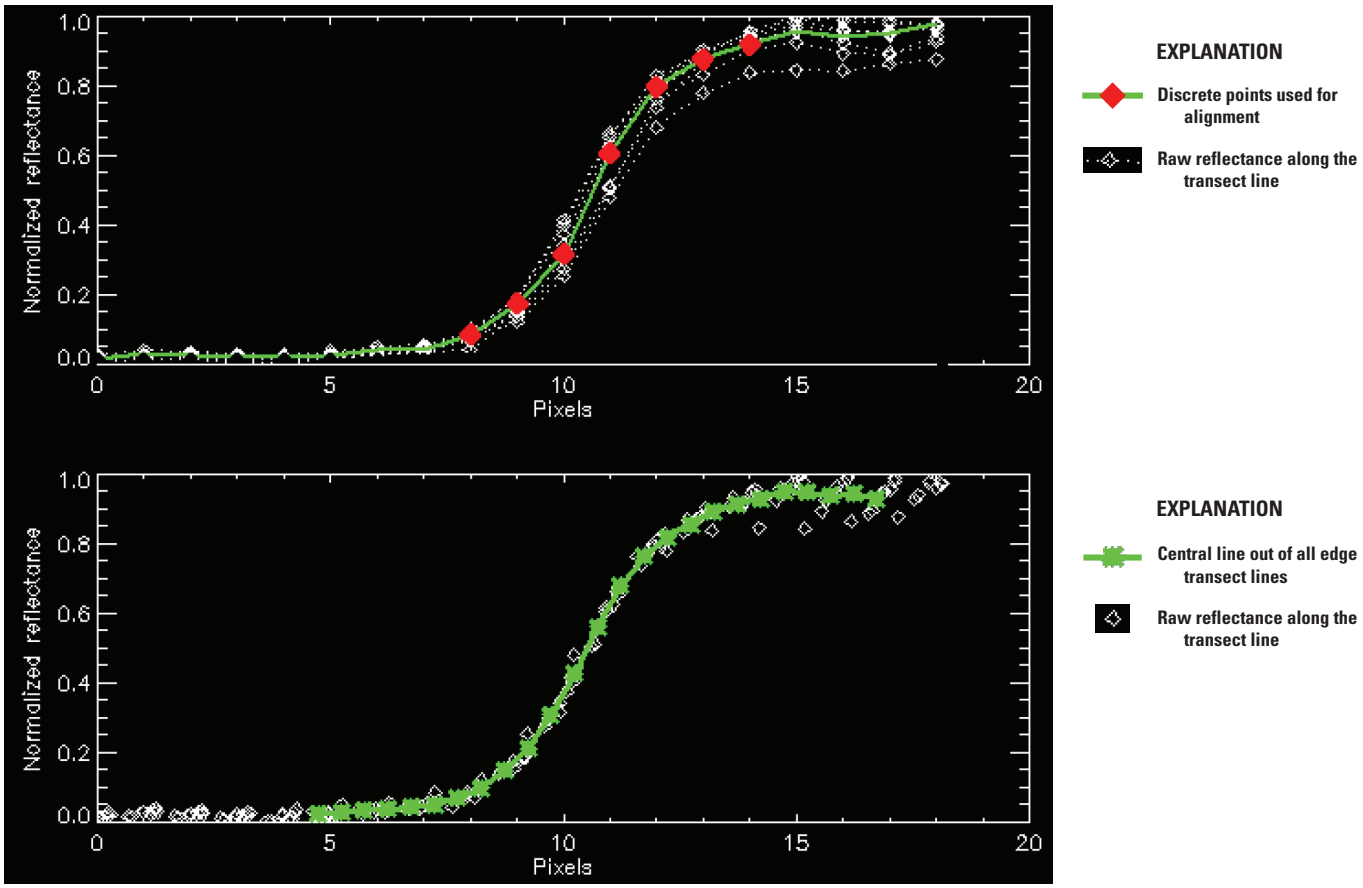

Figure 23. Band 4 (near infrared) raw edge transects (upper) and shifted transects (lower) for Baotou, China.

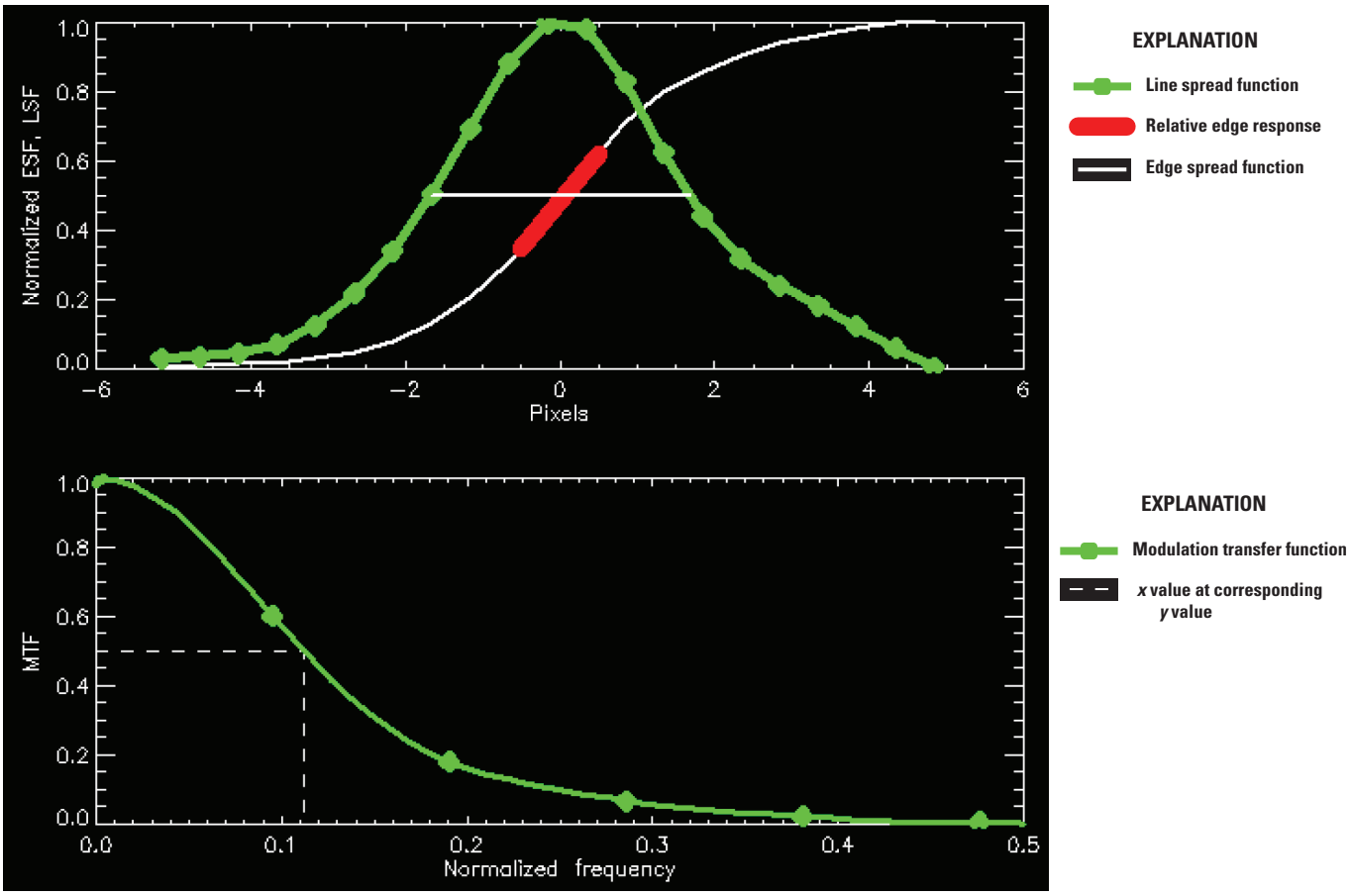

Figure 24. Band 4 (near infrared) edge spread function (ESF) and line spread function (LSF; upper) and modulation transfer function (MTF; lower) for Baotou, China.

Summary and Conclusions

This report summarizes the sensor performance of Planet's Dove Classic system based on the U.S. Geological Survey Earth Resources Observation and Science Cal/Val Center of Excellence (ECCOE) system characterization process. In summary, we have determined that this sensor provides an interior geometric performance in the range of −0.218 (−0.073 pixel) to −0.037 meter (m; −0.012 pixel) in easting −0.167 (−0.056 pixel) to −0.111 m (−0.037 pixel) in northing in band-to-band registration, an exterior geometric error of −6.841 (−2.280 pixels) in easting −6.235 m (−2.078 pixels) in northing offset in comparison to Landsat 8 OLI, a radiometric performance in the range of −0.057 to −0.010 in offset and 0.963 to 1.298 in slope, and a spatial performance in the range of 2.77 to 3.35 pixels for full width at half maximum, with a modulation transfer function at a Nyquist frequency in the range of 0.003 to 0.010.

In conclusion, the team has completed an ECCOE standardized system characterization of the Dove Classic sensing system. Although the team followed characterization procedures that are standardized across the many sensors and sensing systems under evaluation, these procedures are customized to fit the individual sensor as was done with Dove Classic. The team has acquired the data, defined proper testing methodologies, carried out comparative tests against specific references, recorded measurements, completed data analyses, and quantified sensor performance accordingly. The team also endeavored to retain all data, measurements, and methods. This is key to ensure that all data and measurements are archived and accessible and that the performance results are reproducible.

The ECCOE project and associated Joint Agency Commercial Imagery Evaluation partners are always interested in reviewing sensor and remote sensing application assessments and would like to see and discuss information on similar data and product assessments and reviews. If you would like to discuss system characterization with the U.S. Geological Survey ECCOE and (or) the Joint Agency Commercial Imagery Evaluation team, please email us at eccoe@usgs.gov.

Selected References

Planet Labs, Inc., 2021, Planet: Planet Labs, Inc., web page, accessed May 10, 2020, at https://www.planet.com/.

Ramaseri Chandra, S.N., Christopherson, J.B., and Casey, K.A., 2020, 2020 Joint Agency Commercial Imagery Evaluation—Remote sensing satellite compendium (ver. 1.1, October 2020): U.S. Geological Survey Circular 1468, 253 p. [Also available at https://doi.org/10.3133/cir1468.] [Supersedes USGS Circular 1455.]

U.S. Geological Survey, 2020a, EROS CalVal Center of Excellence (ECCOE): U.S. Geological Survey web page, accessed May 10, 2020, at https://www.usgs.gov/core-science-systems/eros/calval.

U.S. Geological Survey, 2020b, Landsat missions—Glossary and acronyms: U.S. Geological Survey web page, accessed May 10, 2020, at https://www.usgs.gov/core-science-systems/nli/landsat/glossary-and-acronyms.

Appendix 1. Radiometric Data

Datasets used for the radiometric stability time-series analysis are listed in table 1.1.

Table 1.1. Radiometric time-series analysis reference datasets.

[OLI, Operational Land Imager; ID, identifier; _02ef, camera identifier; m, meter]

Month	Landsat 8 OLI product ID	Dove Classic ID (_02ef)	Time difference (m)
Apr. 2017	LC08_L1TP_023037_20170408_20170414_01_T1	20170408_160456	33
Apr. 2017	LC08_L1TP_023037_20170408_20170414_01_T1	20170408_160504	33
May 2017	LC08_L1TP_089084_20170524_20170614_01_T1	20170524_231640	26
May 2017	LC08_L1TP_089084_20170524_20170614_01_T1	20170524_231641	26
May 2017	LC08_L1TP_089084_20170524_20170614_01_T1	20170524_231642	26
June 2017	LC08_L1TP_033042_20170601_20170615_01_T1	20170601_171146	29
June 2017	LC08_L1TP_033042_20170601_20170615_01_T1	20170601_171147	29
June 2017	LC08_L1TP_033042_20170601_20170615_01_T1	20170601_171148	29
July 2017	LC08_L1TP_036029_20170708_20170717_01_T1	20170725_172115	32
July 2017	LC08_L1TP_036037_20170708_20170717_01_T1	20170725_172420	33
July 2017	LC08_L1TP_036037_20170708_20170717_01_T1	20170725_172421	33
Aug. 2017	LC08_L1TP_178034_20170828_20170914_01_T1	20170828_080308	30
Aug. 2017	LC08_L1TP_178034_20170828_20170914_01_T1	20170828_080309	30
Sept. 2017	LC08_L1TP_168035_20170923_20171013_01_T1	20170923_070407	29
Oct. 2017	LC08_L1TP_168034_20171025_20171107_01_T1	20171025_070102	30
Oct. 2017	LC08_L1TP_168034_20171025_20171107_01_T1	20171025_070107	30
Oct. 2017	LC08_L1TP_168034_20171025_20171107_01_T1	20171025_070126	30
Nov. 2017	LC08_L1TP_197035_20171121_20171206_01_T1	20171121_100852	24
Nov. 2017	LC08_L1TP_197035_20171121_20171206_01_T1	20171121_100855	24
Nov. 2017	LC08_L1TP_197035_20171121_20171206_01_T1	20171121_100857	24
Dec. 2017	LC08_L1TP_128049_20171220_20171224_01_T1	20171220_030332	28
Dec. 2017	LC08_L1TP_128049_20171220_20171224_01_T1	20171220_030341	28
Dec. 2017	LC08_L1TP_128049_20171220_20171224_01_T1	20171220_030342	28
Jan. 2018	LC08_L1TP_032037_20180120_20180206_01_T1	20180120_170400	29
Jan. 2018	LC08_L1TP_032037_20180120_20180206_01_T1	20180120_170408	29
Jan. 2018	LC08_L1TP_032040_20180120_20180206_01_T1	20180120_170520	29
Jan. 2018	LC08_L1TP_032040_20180120_20180206_01_T1	20180120_170521	29
Feb. 2018	LC08_L1TP_128051_20180206_20180221_01_T1	20180206_030844	23
Feb. 2018	LC08_L1TP_128051_20180206_20180221_01_T1	20180206_030845	23
Feb. 2018	LC08_L1TP_128051_20180206_20180221_01_T1	20180206_030846	23
Mar. 2018	LC08_L1TP_022031_20180303_20180319_01_T1	20180303_160129	26
Mar. 2018	LC08_L1TP_022032_20180303_20180319_01_T1	20180303_160203	25
Apr. 2018	LC08_L1TP_191028_20180420_20180502_01_T1	20180420_093038	20
Apr. 2018	LC08_L1TP_191028_20180420_20180502_01_T1	20180420_093042	20
Apr. 2018	LC08_L1TP_191028_20180420_20180502_01_T1	20180420_093045	20
May 2018	LC08_L1TP_025034_20180527_20180605_01_T1	20180527_162522	22
May 2018	LC08_L1TP_025034_20180527_20180605_01_T1	20180527_162523	22
May 2018	LC08_L1TP_025034_20180527_20180605_01_T1	20180527_162524	22
June 2018	LC08_L1TP_196028_20180626_20180704_01_T1	20180626_100108	20
June 2018	LC08_L1TP_196028_20180626_20180704_01_T1	20180626_100109	20
July 2018	LC08_L1TP_042036_20180721_20180731_01_T1	20180721_180700	26
July 2018	LC08_L1TP_042036_20180721_20180731_01_T1	20180721_180701	26
Aug. 2018	LC08_L1TP_192029_20180817_20180829_01_T1	20180817_093542	22

Table 1.1. Radiometric time-series analysis reference datasets.—Continued

[OLI, Operational Land Imager; ID, identifier; _02ef, camera identifier; m, meter]

Month	Landsat 8 OLI product ID	Dove Classic ID (_02ef)	Time difference (m)
Aug. 2018	LC08_L1TP_192029_20180817_20180829_01_T1	20180817_093553	22
Aug. 2018	LC08_L1TP_192029_20180817_20180829_01_T1	20180817_093554	22
Sept. 2018	LC08_L1TP_200026_20180926_20181009_01_T1	20180926_102341	24
Sept. 2018	LC08_L1TP_200026_20180926_20181009_01_T1	20180926_102346	24
Sept. 2018	LC08_L1TP_200027_20180926_20181009_01_T1	20180926_102358	24
Sept. 2018	LC08_L1TP_200027_20180926_20181009_01_T1	20180926_102359	24
Oct. 2018	LC08_L1TP_025030_20181018_20181031_01_T1	20181018_162115	24
Oct. 2018	LC08_L1TP_025030_20181018_20181031_01_T1	20181018_162119	24
Oct. 2018	LC08_L1TP_025031_20181018_20181031_01_T1	20181018_162137	26
Oct. 2018	LC08_L1TP_025031_20181018_20181031_01_T1	20181018_162146	26
Nov. 2018	LC08_L1TP_023034_20181121_20181129_01_T1	20181121_161104	25
Nov. 2018	LC08_L1TP_023034_20181121_20181129_01_T1	20181121_161109	25
Nov. 2018	LC08_L1TP_023034_20181121_20181129_01_T1	20181121_161117	25
Dec. 2018	LC08_L1TP_016040_20181222_20181227_01_T1	20181222_153224	22
Dec. 2018	LC08_L1TP_016040_20181222_20181227_01_T1	20181222_153225	22
Dec. 2018	LC08_L1TP_016040_20181222_20181227_01_T1	20181222_153233	22
Jan. 2019	LC08_L1TP_091085_20190120_20190201_01_T1	20190120_234405	11
Jan. 2019	LC08_L1TP_091085_20190120_20190201_01_T1	20190120_234418	11
Feb. 2019	LC08_L1TP_041036_20190207_20190221_01_T1	20190207_180954	18
Feb. 2019	LC08_L1TP_041036_20190207_20190221_01_T1	20190207_180955	18
Feb. 2019	LC08_L1TP_041036_20190207_20190221_01_T1	20190207_180956	18
Mar. 2019	LC08_L1TP_180032_20190325_20190403_01_T1	20190325_082920	16
Mar. 2019	LC08_L1TP_180032_20190325_20190403_01_T1	20190325_082925	16
Mar. 2019	LC08_L1TP_180033_20190325_20190403_01_T1	20190325_083005	15
Mar. 2019	LC08_L1TP_180033_20190325_20190403_01_T1	20190325_083006	15

For more information about this publication, contact:
Director, USGS Earth Resources Observation and Science Center
47914 252nd Street
Sioux Falls, SD 57198
605–594–6151

For additional information, visit: https://www.usgs.gov/centers/eros

Publishing support provided by the
Rolla Publishing Service Center

ISSN 2331-1258 (online)
https://doi.org/10.3133/ofr20211030C